Current-Mode Approach in Power Supplies for DBD Excilamps: Review of 4 Topologies

Rafael Diez, Hubert Piquet, David Florez, Xavier Bonnin

Current-Mode Approach in Power Supplies for DBD Excilamps: Review of 4 Topologies

Rafael Diez, *Member, IEEE*, Hubert Piquet, David Florez, *Member, IEEE*, and Xavier Bonnin

***Abstract*— This document reviews the current-mode supply approach for dielectric barrier discharge (DBD) excilamps. It briefly demonstrates why this mode assures the control of the power injected into the DBD. Considerations with the step-up transformer required for the correct operation of the current-mode are developed. This document shows and compares four different converter topologies that comply with this principle. This comparison is made in terms of electric efficiency and luminous efficacy using experimental measurements.**

***Index Terms*— Current control, dielectric barrier discharge (DBD), power conversion, ultraviolet (UV) generation.**

I. Introduction

THE ultraviolet (UV) radiation used in different applications, such as skin diseases treatment, water sterilization, microlithography, and surface cleaning [1]–[5], is generally generated using mercury-based lamps (medium and low pressures). Among the alternatives for UV sources, it is possible to find the LEDs, which are still very low power [6] or only dedicated to the UV-A range [7], and finally the excimer or exciplex lamps, here called excilamps.

The excilamps present numerous advantages, as the fact that no mercury is used in their gas mixture, their radiation is confined in a very narrow band and the emission wavelength can be selected as a function of the gas composition. In addition, their lifetime is longer than those of the mercury-based lamps, thanks to the dielectric barrier discharge (DBD) construction [8]. In the present, there are some studies trying to validate the efficacy of the excilamps over the mercury-based lamps [9].

The UV radiation from the DBD excilamps was studied in the beginning only from the point of view of the physics, and some characteristics, for instance the duration of the UV pulses, were not directly related with the power supply [10]. These discharges were created using general-purpose linear power amplifiers or pulsed-mode voltage converters [11]–[13].

Actually, in [14] and [15], some parameters of the UV radiation, like the duration and amplitude, have been demonstrated to be controlled by the current injected into the lamp, by means of a current-mode converter.

Resonant topologies controlling the current are now frequently used to deliver the power to DBD loads [16]–[19].

This paper revises the current-mode approach origin for DBD lamps, including the modeling of an excilamp. It has a view of four different converter structures that comply with this approach, and finally, a comparison of those structures is made in terms of electric efficiency and luminous efficacy. Practical considerations in the construction of the transformer, necessary for all the converters, are developed.

II. Review of the Current-Mode Approach

In this section, the development of the current-mode approach is summarized. The characterization of the static and dynamic electric behavior of the load, by means of a model, is the starting point, which allows the selection of the adequate fundamental properties of the supplies.

The latter must be able to control the energy and the power injected into the lamp, and it is obtained by means of a static converter specifically designed for this task.

A. Electrical Model

The electrical model for a DBD excilamp can be generally drawn as the typical circuit used to represent other DBDs [20], [21], as shown in Fig. 1, where C_d stands for the equivalent series capacitance of the dielectric barriers containing the gas mixture; C_g represents the gas dielectric behavior before breakdown; and G_g characterizes the gas conductance as a function of the gas voltage v_g.

In [22], it was demonstrated that the model can be simplified to achieve the design of the power supply of the lamp, considering that v_g is almost constant once the discharge is established

$$\begin{aligned} v_g &\cong +V_{\text{th}}, \quad \text{if} \quad i_g > 0 \\ v_g &\cong -V_{\text{th}}, \quad \text{if} \quad i_g < 0 \end{aligned} \tag{1}$$

R. Diez is with the Department of Electronic Engineering, Pontificia Universidad Javeriana, Bogotá 11001000, Colombia (e-mail: rdiez@javeriana.edu.co).

H. Piquet and X. Bonnin are with the Laboratoire Plasma et Conversion d'Energie, Centre National de la Recherche Scientifique, Institut National Polytechnique de Toulouse, Université de Toulouse, Toulouse F-31062, France (e-mail: hubert.piquet@laplace.univ-tlse.fr; xavier.bonnin@laplace.univ-tlse.fr).

D. Florez was with the Department of Electronic Engineering, Pontificia Universidad Javeriana, Bogotá 11001000, Colombia, and also with the the Laboratoire Plasma et Conversion d'Energie, Centre National de la Recherche Scientifique, Institut National Polytechnique de Toulouse, Université de Toulouse, Toulouse F-31062, France. He is now with the Escuela de Ciencias Exactas e Ingeniería, Universidad Sergio Arboleda, Bogotá 11001000, Colombia (e-mail: david.florez@usa.edu.co).

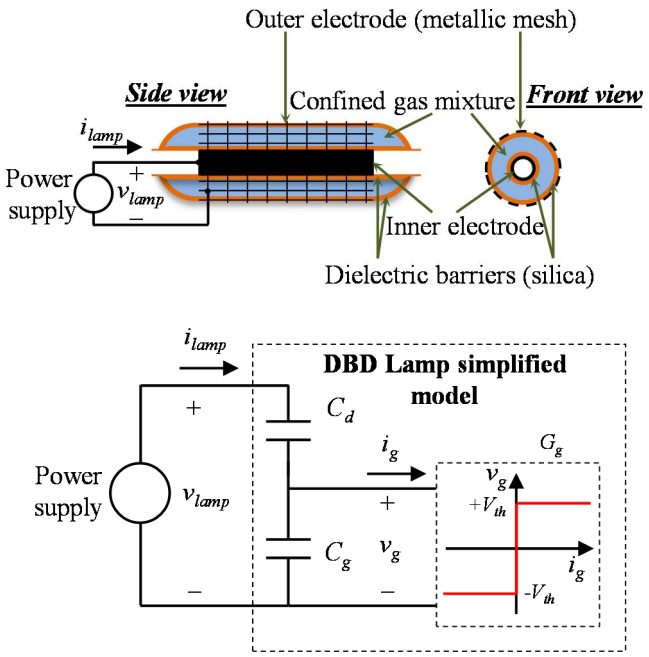

Fig. 1. DBD excilamp. Physical structure (top) and equivalent electric model (bottom).

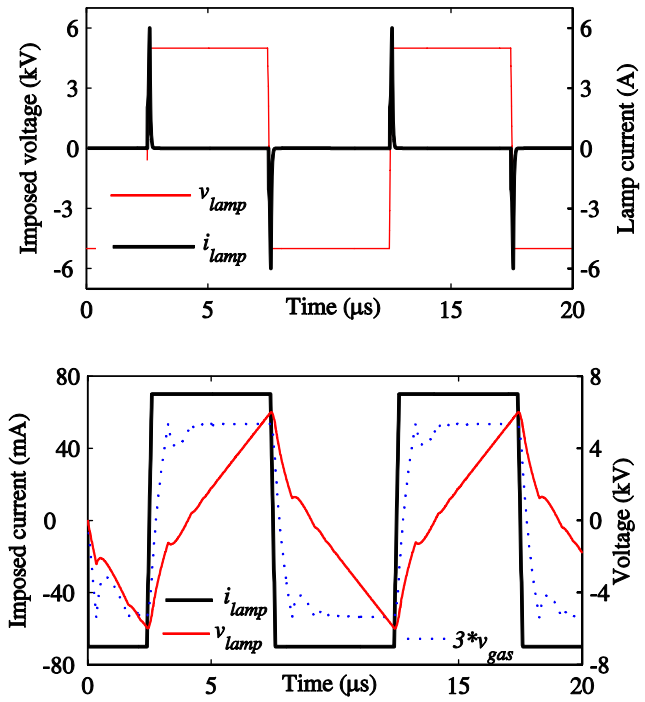

Fig. 2. Voltage-mode converter with square voltage output and uncontrolled current (top), and current-mode converter with square current and controlled voltage (bottom). Gas voltage is almost constant after breakdown.

where i_g is the gas current and V_{th} is a constant voltage value here called the normal gas voltage. This constant voltage means that the discharge could be treated as being in the normal glow regime.

Nevertheless, if more precise waveforms for the electric variables must be obtained, the model containing the dynamic evolution of the conductance is considered [22].

B. Current Mode Versus Voltage Mode

The simplified electrical model emphasizes two reasons why a DBD excilamp should be supplied with a current source. The first one is the capacitive nature of the lamp: a voltage source converter would inject a lamp current i_{lamp} only in case of a variation in the lamp voltage v_{lamp}, as revealed in (2). In this case, the waveform of i_{lamp} current is difficult to predict in amplitude and duration, as can be seen for a square-voltage source converter in Fig. 2

$$i_{\text{lamp}} = C_d \cdot \frac{\mathrm{d}(v_{\text{lamp}} - v_g)}{\mathrm{d}t}. \tag{2}$$

Conversely in a current-mode converter, as i_{lamp} is imposed, the lamp voltage is computed using (3). In this case, it is possible to calculate during the design stage all the electrical variables in the converter, and this guarantees a good dimensioning of the power supply (Fig. 2)

$$v_{\text{lamp}} = v_g + \frac{1}{C_d} \int i_{\text{lamp}}\, \mathrm{d}t. \tag{3}$$

The second reason to use a current-mode converter is that once the discharge is established in the gas, v_g can be considered constant (Fig. 2). In consequence, the current of the gas capacitance can be neglected and the gas current i_g (in the conductance) will be equal to the injected lamp current i_{lamp}.

Since the instantaneous power in the gas is governed by i_g (4), so will be the average power of the lamp P_{lamp}. Indeed, G_g gas conductance is the only dissipative element in the DBD lamp equivalent circuit (Fig. 1)

$$p_g = V_{\text{th}} * |i_g|. \tag{4}$$

Note that for current-mode converters, the gas power is independent from the dielectric equivalent capacitance. This is not true for the voltage-mode converters, as the lamp current depends on the applied voltage (2).

C. Choice of the Injected Current

Considered the fact that the instantaneous power dissipated in the discharge p_g is directly controlled by the gas current i_g, the lamp current i_{lamp} shown in Fig. 3 is proposed to supply the DBD load. It is possible to see that the gas voltage v_g takes a determined time t_{th} to invert its polarity and to reach the breakdown between positive and negative half-cycles.

The p_g waveform is obtained with (4), then its average value is computed to obtain the average power of the lamp P_{lamp} [14]

$$P_{\text{lamp}} = J \cdot D \cdot V_{\text{th}} - 4 f_{\text{lamp}} C_{\text{eq}} V_{\text{th}}^2 \tag{5}$$

where C_{eq} is the series equivalent capacitance of C_d and C_g. With this i_{lamp} waveform, it is possible to control and adjust P_{lamp} with three degrees of freedom: the current amplitude J, the operating frequency f_{lamp}, and the duty ratio D. The implementation of a converter that is able to produce this current waveform is developed in the following section.

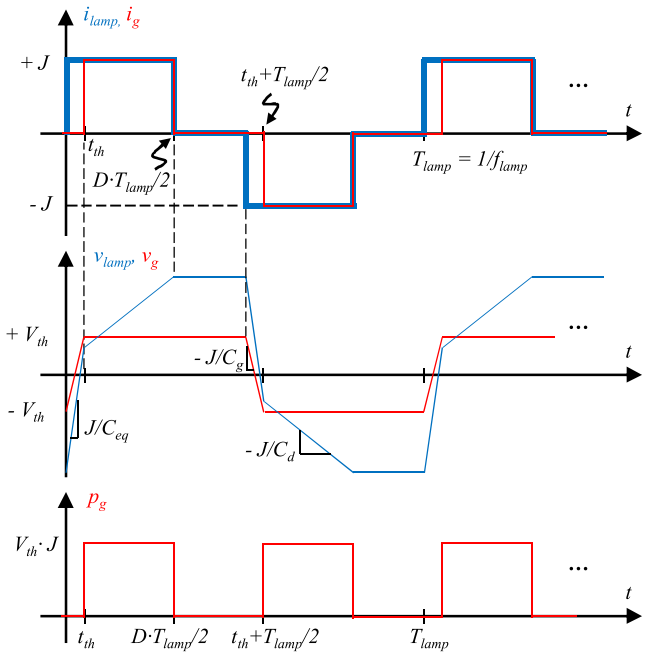

Fig. 3. Rectangular lamp current waveform supplying the DBD lamp.

III. Converter Topologies

In this part, four different topologies for current-mode converters are presented. The first one obtains the rectangular current waveform presented in the previous section. The other three topologies are resonant-based structures, exhibiting different lamp current shape, but assuring the control of the lamp power, since those are also based on the current injection to the lamp.

A. Rectangular Current Converter

This structure is conceived as a constant current source in cascade with a current inverter, as shown in Fig. 4. The amplitude of current J is controlled by the current source using a hysteretic control. The duty cycle and frequency of the lamp current are set by means of the inverter. The current source is built with a two-quadrant chopper, considering that bipolar voltage is found at the input of the inverter. This chopper works in Continuous Conduction Mode (CCM). A full bridge, composed by high-frequency synthesized thyristors [23], is used as the current inverter, to give the necessary degrees of freedom to the power supply. For the control of the lamp current shape (Fig. 3), the sequence used for the inverter switches is shown in Fig. 4 (bottom). A step-up transformer is necessary to scale the high voltage of the lamp to the range of the high-frequency semiconductors. Details about this structure are found in [24] and [25].

The power delivered to the lamp is computed with (5). This structure is the most flexible among the converters listed in this paper; it can control the power of the lamp via three independent variables (degrees of freedom: D, J, and f_{lamp}), for this reason, it is very useful for the identification of the optimal operating point of the load. Nevertheless, this converter is not optimized in terms of

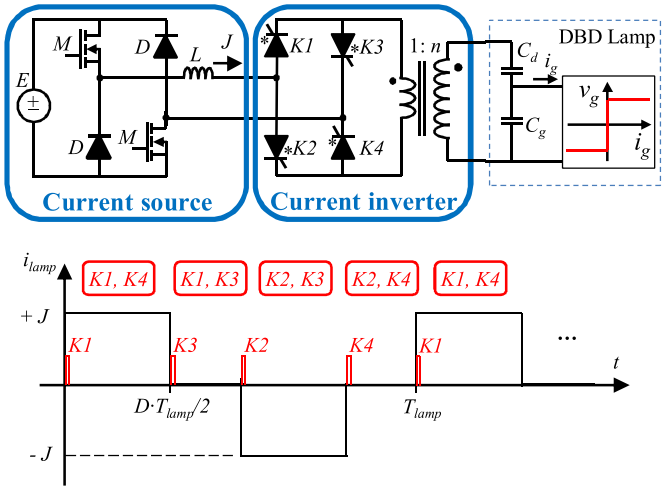

Fig. 4. Rectangular current converter offering three degrees of freedom to adjust the lamp current and hence the lamp power, with the trigger sequence for the high-frequency thyristors in the inverter.

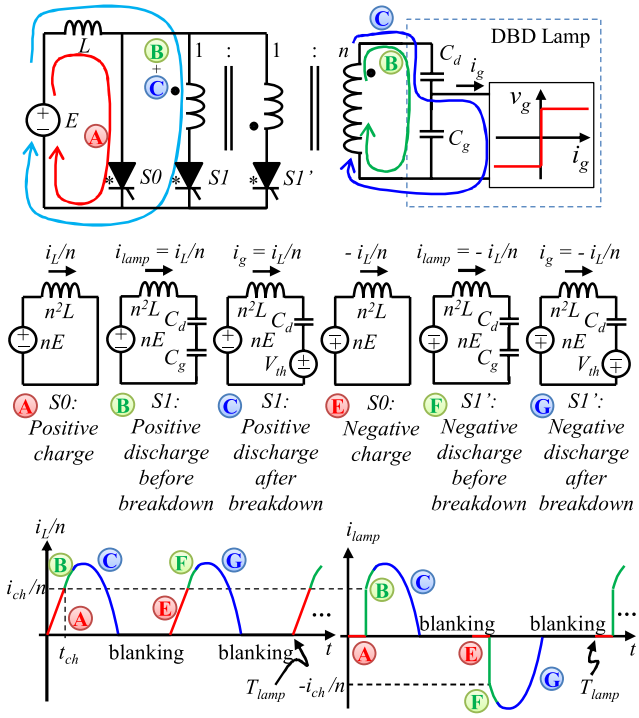

Fig. 5. Boost-based converter structure, its six operating sequences as seen in the secondary and the current waveforms.

electrical efficiency or cost, since it uses a big number of switches, part of them presenting hard-commutation conditions.

B. Boost-Based Converter

This structure, introduced in [26], uses a boost converter, working in Discontinuous Conduction Mode (DCM), to replace the two-quadrant chopper from previous configuration. In DCM, the current inverter can be replaced by a push–pull inverter, using a two-primary-winding transformer, reducing the number of switches and the control circuitry, as observed

in Fig. 5. One can note that all switches are thyristor-like devices, according to the double polarity of v_{lamp} [27].

The inductance current presents, for the positive half-cycle, three different sequences: linear increase of the inductance current to i_{ch} (S0 ON), resonant discharge (S1 ON), and blanking (all switches OFF). These sequences are repeated for the negative half-cycle, inverting the current direction, using S1′ instead of S1, to comply with the charge balance required supplying this capacitive load. The duration of the discharge sequence is defined by the values of the components and by the value of the inductance current at the end of the charge sequence (i_{ch}). The blanking time sets the operating frequency.

The resonant discharges can be separated in two: before and after breakdown and the equivalent resonance capacitance are C_{eq} and C_d, respectively. The first resonant part, when the gas current is zero, should be minimized to obtain a gas current similar to the imposed lamp current.

The power delivered to the lamp (6) is calculated using the positive sequence, taking the average of the gas current and then multiplying by the constant gas voltage V_{th}. Finally, this value is doubled to consider both the negative and positive sequences

$$P_{\text{lamp}} = \frac{f_{\text{lamp}} V_{\text{th}} \left(\dfrac{E^2 \cdot t_{\text{ch}}^2}{L} + 4nEV_{\text{th}}C_g \right)}{V_{\text{th}} - nE}. \tag{6}$$

Being t_{ch}, the time that the input voltage (E) linearly charges the inductance (L) to the i_{ch} value.

This expression states that stability for this converter is assured by maintaining the input voltage seen in the secondary nE less than the V_{th} voltage. Otherwise, divergent developments for voltage and current are found [28].

The end of the discharge phase in this converter is established by the spontaneous turn-OFF of one of the two inverter switches with Zero-Current Switching (ZCS).

C. Buck–Boost-Based Converter

This converter, using a buck–boost in DCM as the unidirectional current source, has similar charge and discharge sequences as the boost-based converter (Fig. 6).

This converter works as a bidirectional current flyback converter, as detailed in [28]. The energy stored in the inductance, during the charge phase, is sent to the lamp during the discharge phase. In this way, the power delivered to the lamp can be easily computed as (assuming 100% efficiency of the converter)

$$P_{\text{lamp}} = \frac{f_{\text{lamp}}}{L}(E \cdot t_{\text{ch}})^2. \tag{7}$$

As for the boost-based converter, the buck–boost-based structure can vary the output power adjusting the charge time t_{ch}, the input voltage E, and the operating frequency f_{lamp}. However, current amplitude and duration are not independent variables in these converters as it was for the rectangular current converter.

Differing from the boost-based topology, the buck–boost converter is stable for all the values of the input voltage, as demonstrated in [29]. Here, ZCS is also assured at the end of the discharge sequence.

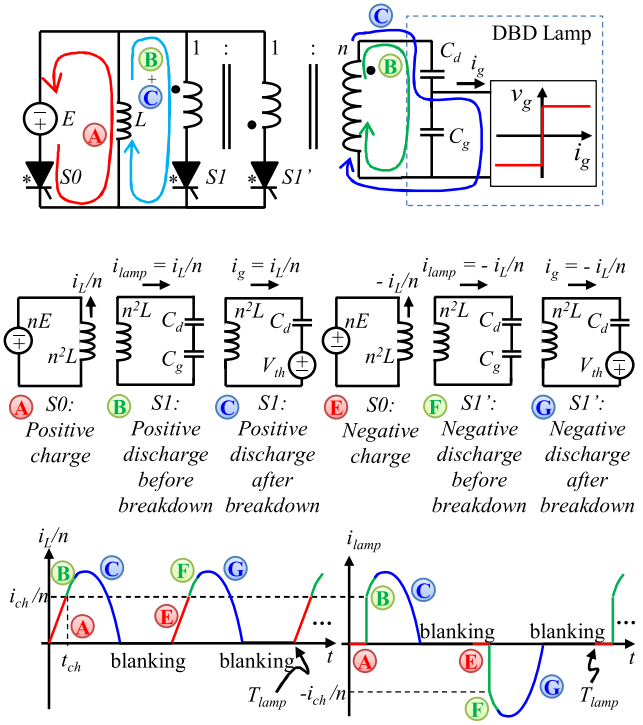

Fig. 6. Structure of the buck–boost-based converter. Its six operating sequences as seen in the secondary, and the inductor and output current.

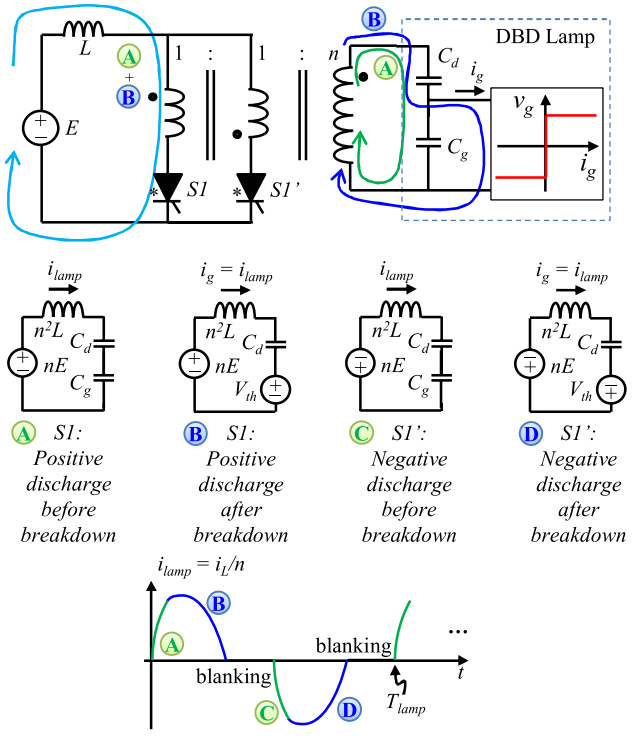

Fig. 7. Series resonant inverter topology. Its four operating sequences and its output current waveform.

TABLE I
PARAMETERS OF THE EXCILAMP USED DURING IMPLEMENTATION

V_{th}	C_d	C_g	*Power rating*	*Typical operating Frequency range*
1300 V	110 pF	40 pF	100 W	40-100 kHz

D. DCM Operated Series Resonant Inverter

This structure, shown in Fig. 7, is a simplification of the boost-based topology. Here, no charge sequence is allowed; hence, only discharge and blanking phases are presented.

As for the boost-based converter, the input voltage seen in the secondary must be less than the normal voltage of the gas V_{th}; otherwise, unstable situation occurs.

The power delivered to the lamp is calculated in the same way as for boost-based topology, as demonstrated in [30]

$$P_{\text{lamp}} = 4 f_{\text{lamp}} {V_{\text{th}}}^2 C_g \left(\frac{nE}{V_{\text{th}} - nE} \right). \tag{8}$$

Here, the parameters that can be controlled to adjust the lamp power are only the operating frequency f_{lamp} and the input voltage E.

Concerning the advantages, this topology can be implemented with only two switches and it presents ZCS during turn-OFF and also at turn-ON, making it the least expensive and most efficient topology.

IV. IMPLEMENTATION AND EXPERIMENTAL RESULTS

In this section, the implementation of the four structures is made for the same load: a XeCl (308 nm) lamp with the following parameters.

As the parameters, corresponding to the normal gas voltage V_{th}, the dielectric capacitance, and the gas capacitance, are considered constant for one lamp, the peak voltage of this lamp (9) is only dependent on the lamp power and the lamp frequency, as demonstrated in [24]

$$v_{\text{lamp\_peak}} = \frac{P_{\text{lamp}}}{4 f_{\text{lamp}} V_{\text{th}} C_d} + V_{\text{th}} \left(1 + \frac{C_g}{C_d + C_g} \right). \tag{9}$$

That means that for all the four converters the peak voltage could be as high as 5000 V for the low-frequency operation. To reduce this voltage to the semiconductor range, a step-up transformer with 1:10 ratio is designed.

A. Step-Up Transformer Design

The high-voltage transformer strongly impacts the converter performance and the delivered waveforms through its parasitic elements [31], [32]; for this reason, special attention should be paid to capacitive couplings among the transformer windings.

Assuming high coupling in the transformer, these capacitive links can be encompassed into a single parasitic capacitor connected in parallel to the secondary side [32], forming a capacitive current divider with the low structural DBD capacitances (Table I). Therefore, this capacitance has to be minimized.

TABLE II
COMPARISON OF THREE TRANSFORMERS

	Ns	*Nl*	*Nt*	*n*	*Cp*	*Lm*	*Rc*	*Ri*
T1	1	1	~260	10	11 pF	400 mH	1	1
T2	1	2	~520	10	25 pF	1200 mH	~2	~2
T3	2	2	~520	10	14 pF	1200 mH	~2	~2

Furthermore, the theoretical waveforms presented in Section III might be altered if the magnetizing inductance of the transformer (which is also connected in parallel with the load) presents an extremely low value.

Finally, it is important to bear in mind that transformer efficiency might be reduced if losses are not carefully considered.

These issues can be addressed by carefully winding the transformer and inserting thick enough low-permittivity insulation materials between the winding layers and the magnetic core. Single-layer windings are of major interest in that regard, since the interlayer capacitive coupling term is eliminated [31]. Nevertheless, tradeoff with losses, weight, and magnetizing inductance has to be made, and it appears that a multilayer winding widens the field of possibilities.

As stated in [32], splitting the secondary in several sections connected in series (N_s) leads to the reduction of capacitive effects, while increasing the number of layers (N_l) and turns (N_t) at the secondary winding.

To show this, three *Ferroxcube E80/38/20-3F3* core based transformers have been manufactured according to the lamp parameters given in Table I and experimentally compared in Table II.

The turns ratio n is chosen to be 10 to bring back a voltage that the power switches can withstand. The R_c and R_i parameters, respectively, stand for the copper and iron resistances, both normalized with respect to those of the transformer T1.

L_m and C_p, respectively, denote the magnetizing inductance and the parasitic capacitance seen in the secondary side of the transformer. The insulation materials are acrylic layers, with 4.5-mm thickness between primary and secondary, and 2 mm between the secondary layers. The sections of T3 are also separated with a 2-mm acrylic layer. As predicted, the single layer transformer (T1) offers the best capacitive behavior.

To increase the magnetizing inductance by 4 with respect to T1, T2 transformer uses a classical two-layer winding in the secondary; however, it suffers from an important electrostatic coupling term (increased by a factor 2.27 compared with T1).

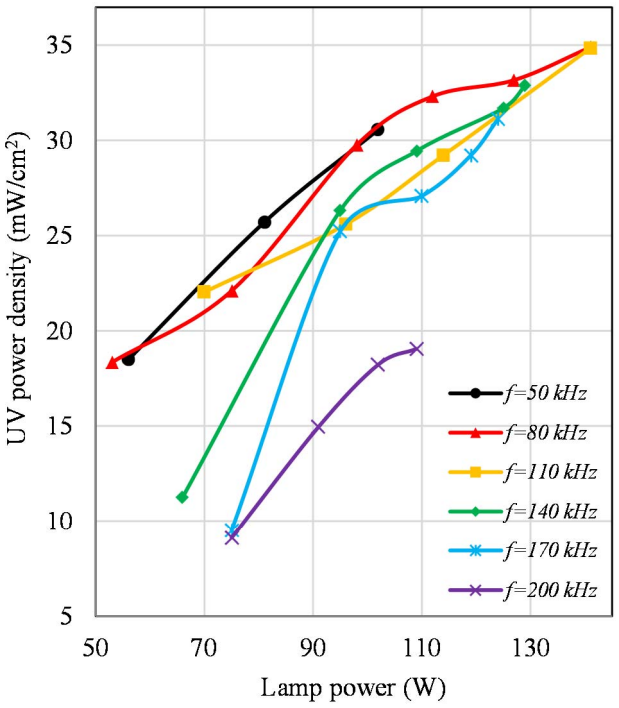

Fig. 8. Example of the optimal operating point identification using the rectangular current converter. For a fixed injected power in the lamp, the UV power density depends on the operating frequency.

Finally, T3 transformer offers an interesting compromise by increasing L_m by the same factor 4 and only increasing C_p by 1.25. For T2 and T3, R_c and R_i are approximately increased by a factor 2.

These results show that increasing the number of layers and splitting the winding gives a degree of freedom to distribute copper and iron losses and to reach desired values in term of magnetic parameters, and still guaranteeing an interesting value for C_p.

B. Exploitation of the Degrees of Freedom to Identify the Optimum Operating Point in Terms of Luminous Efficacy

Beyond the capability of controlling the lamp power, the current-mode converters are capable of adjusting the power in different forms. In this aspect, the rectangular current converter is the most versatile, being the only converter capable of varying independently, and during operation, the three degrees of freedom of the injected lamp current and hence the instantaneous lamp power: magnitude, duration, and frequency.

For this reason, this converter can be used to identify an optimal operating point of the lamp, where the luminous efficacy is maximized, within the range of the converters; one example of this is shown in Fig. 8. To obtain this figure, the current amplitude in the lamp is kept constant (128 mA), the frequency is fixed, and the duty cycle is adjusted to obtain different average powers delivered to the lamp. After sweeping the duty-cycle range, the operating frequency is changed, and the procedure is repeated until the power range is covered [14].

For this and other experiments in this paper, the UV average radiation is measured with an optometer GIGAHERTZOPTIK P-9710 and the UV detector SN5816, installed at 3 mm of the lamp surface.

For instance, in this figure, it is possible to see that if we desire a UV power density around 30 mW/cm^2, the necessary power to be injected to the lamp is much lower if the operating frequency is between 50 and 80 kHz. In this range, a luminous efficacy gain of 30% is achieved comparing with the 170 kHz.

C. Comparison of the Converters

Once the optimal operating point is identified with the rectangular converter, it is necessary to design an efficient converter to supply the lamp and hence obtain an overall optimized efficiency. In this paper, a comparison of the four structures is proposed for the following conditions:

1) $P_{\text{lamp}} = 106$ W;
2) $f_{\text{lamp}} = 60$ kHz;
3) discharge time of 3 μs, corresponding to $D = 36\%$.

Fig. 9 shows the different behavior of the four converters, focusing on the current injected into the lamp i_{lamp} and on the UV emitted by the lamp. The duration and shape of the UV pulses are very similar to those of the gas current, governed by the imposed lamp current, as predicted by the current-mode approach.

The UV waveform is in arbitrary units and is obtained with a photodetector THORLABS PDA-25K, configured in the 20-dB gain setting. The detector is oriented perpendicular to the lamp, placing its active area at 25 mm of the lamp surface.

To remark that the lamp peak voltage is similar in the four structures, as predicted by (9). Note that, in the four structures, the lamp voltage waveform is similar and the UV radiation waveform is different. It confirms how difficult would be to control the UV radiation by means of a voltage-mode supply.

1) Electric Efficiency: Table III compares the four topologies: for the same power injected in the lamp, the power at the input of each converter is measured (P_{in}). The transformer is the same for all the structures and the power at its input port, P_{prim}, is similar and around 124 W for the four converters, giving losses near 15% in this element. Note that the transformer is the element with the highest losses for the resonant-based topologies.

Regarding the losses in the converter (semiconductors and inductor), it is possible to see that the rectangular converter presents the highest, with only 55% of efficiency, since it is fully hard switched and because the current flows continuously through the inductance and the switches. This is followed by the buck–boost converter (79% efficiency), as its initial current during the discharge phase is the highest, and so the S1 (or S1') turn-ON losses. The most efficient converter is the series resonant inverter, since it is completely ZCS, presenting 83% of efficiency (97% in the primary side circuit and 86% in the transformer).

2) Luminous Efficacy Depends on Current Waveform: The luminous efficacy is calculated as the output power density divided by the average power, measured at the lamp terminals. It is noticeable that it depends on the current shape, since the electrical lamp power is the same for all the structures, as well as the duration and energy of each pulse. In this

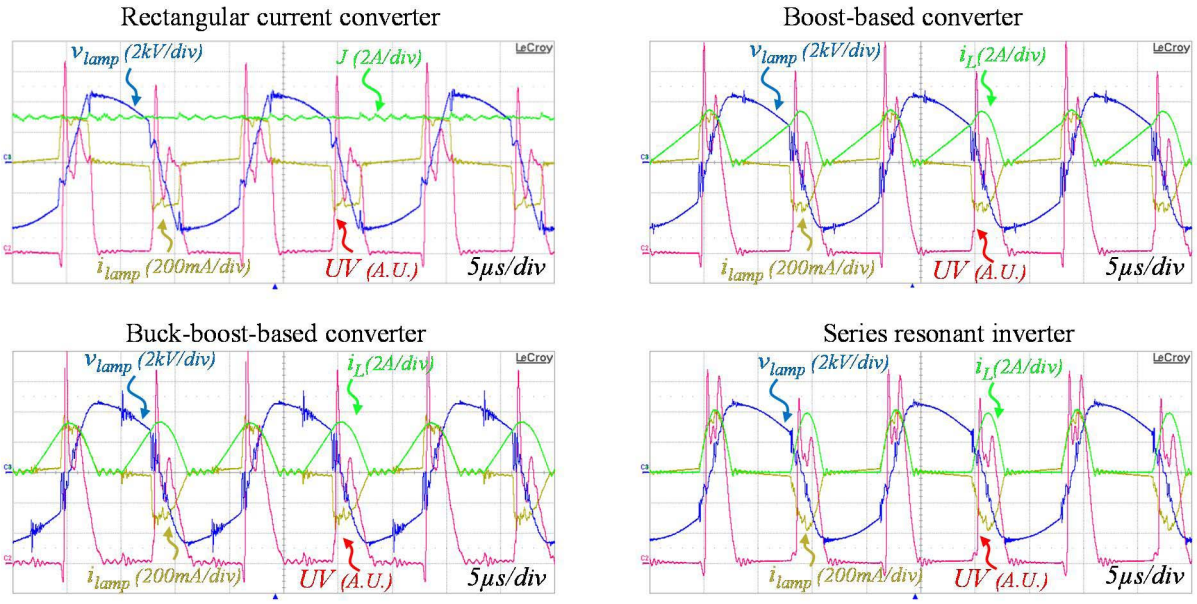

Fig. 9. Experimental waveforms for the four converters under the same power, frequency, and discharge time. Lamp peak voltage is not dependent of the waveform. ZCS can be observed in the inductance current for the resonant-based topologies.

TABLE III
COMPARISON OF THE CONVERTERS

Converter	E (V)	P_{in} (W)	P_{prim} (W)	P_{lamp} (W)	*UV power density* (mW/cm^2)	*Luminous efficacy* (mW/(cm^2·W))	*Overall efficiency* ((mW/(cm^2·W))
Rectangular current	160	194	125	106	28.3	0.267	0.146
Boost based	79	132	123	106	25.3	0.238	0.192
Buck-boost based	246	134	123	106	26.8	0.253	0.200
Series Resonant	137	128	124	106	27.5	0.259	0.215

aspect, the most efficient would be the rectangular current shape obtaining 3.1%, 5.5%, and 12.2%, more compared with the series resonant inverter, buck–boost-based converter, and boost-based converter, respectively.

3) Efficiency for the Entire System: Even though the rectangular converter provides the best luminous efficacy, it presents the worst overall efficiency, which is calculated as the output power density divided by the average power measured at the terminals of the main power source (E). In this term, thanks to its high electric efficiency, the series resonant inverter operated in DCM, presents a gain of 7.5%, 12%, and 47.2%, with respect to the buck–boost-based, boost-based, and rectangular converters, respectively.

4) Other Considerations: In terms of control of the discharge power, the buck–boost-based structure is useful for applications where a very precise constraint of the injected power is necessary or in a situation where the DBD has not been completely identified. In these cases, the charging sequence can be adjusted to increase the output power in the DBD process. It has the advantage of being always stable, while maintaining in DCM.

Finally, Table III shows that input voltage (E) must be different in the three resonant-based topologies, to obtain the same operating conditions. Note that the boost-based converter is the one with the lowest input voltage, making it worthy for applications where low input voltage is available as the main power source, like in photovoltaic and other battery-based systems.

V. CONCLUSION

The current-mode approach to supply the DBD excimer lamps ensures the control of the lamp power and hence the UV power output. Among the four structures revised in this paper, the rectangular current converter has the ability to identify the optimal operating conditions, making it easier to define the electrical parameters to supply the lamp: average power, operating frequency, and discharge duration (or duty cycle).

Once the operating point has been chosen, other three structures have demonstrated to be more efficient than the rectangular current converter and the choice of one among those depends on several aspects: for accurate control of the

injected power and stability the buck–boost-based topology is the best. For low-voltage input, the boost-based converter can be designed to connect directly to the main power source. Finally, the series resonant inverter presents the best efficiency and soft commutation, and it is the cheapest.

REFERENCES

[1] T. Mudigonda, T. S. Dabade, and S. R. Feldman, "A review of targeted ultraviolet B phototherapy for psoriasis," *J. Amer. Acad. Dermatol.*, vol. 66, no. 4, pp. 664–672, Apr. 2012.

[2] R. Brandenburg *et al.*, "Antimicrobial effects of UV and VUV radiation of nonthermal plasma jets," *IEEE Trans. Plasma Sci.*, vol. 37, no. 6, pp. 877–883, Jun. 2009.

[3] X. Wang, X. Hu, H. Wang, and C. Hu, "Synergistic effect of the sequential use of UV irradiation and chlorine to disinfect reclaimed water," *Water Res.*, vol. 46, no. 4, pp. 1225–1232, Mar. 2012.

[4] L. Xu, J. Deng, and M. Wang, "Different phenomena in UV-induced surface flashover," *IEEE Trans. Plasma Sci.*, vol. 40, no. 12, pp. 3508–3511, Dec. 2012.

[5] M. Sakai *et al.*, "Reduction of fluid friction on the surface coated with TiO_2 photocatalyst under UV illumination," *J. Mater. Sci.*, vol. 47, no. 23, pp. 8167–8173, Dec. 2012.

[6] S. Natarajan, Y. Habtemichael, and S. Graham, "Thermal metrology techniques for UV LED light sources," in *Proc. 13th IEEE Intersoc. Conf. Thermal Thermomech. Phenomena Electron. Syst. (ITherm)*, May/Jun. 2012, pp. 314–324.

[7] P.-M. Tu *et al.*, "Study of efficiency droop in InGaN-based near-UV LEDs with quaternary InAlGaN barrier," in *Proc. 10th IEEE Int. Conf. Semicond. Electron. (ICSE)*, Sep. 2012, pp. 418–421.

[8] J.-Y. Zhang and I. W. Boyd, "Lifetime investigation of excimer UV sources," *Appl. Surf. Sci.*, vol. 168, nos. 1–4, pp. 296–299, Dec. 2000.

[9] M. M. Guivan, T. Kamikozawa, H. Kurokawa, H. Motomura, K. Kadowaki, and M. Jinno, "Comparative inactivation of Bacillus subtilis spores using a DBD-driven xenon iodide excilamp and a conventional mercury lamp," *IEEE Trans. Plasma Sci.*, vol. 38, no. 8, pp. 1972–1977, Aug. 2010.

[10] S. Liu and M. Neiger, "Double discharges in unipolar-pulsed dielectric barrier discharge xenon excimer lamps," *J. Phys. D, Appl. Phys.*, vol. 36, no. 13, p. 1565, 2003.

[11] R. P. Mildren, R. J. Carman, and I. S. Falconer, "Visible and VUV emission from a xenon dielectric barrier discharge using pulsed and sinusoidal voltage excitation waveforms," *IEEE Trans. Plasma Sci.*, vol. 30, no. 1, pp. 192–193, Feb. 2002.

[12] A. BenMoussa, A. Belasri, F. Ghaleb, and Z. Harrache, "Gas heating phenomenon in rare gas dielectric barrier discharge for excimer lamps," *IEEE Trans. Plasma Sci.*, vol. 42, no. 3, pp. 706–711, Mar. 2014.

[13] H. Loukil, A. Belasri, K. Khodja, and Z. Harrache, "Theoretical kinetics investigation of xenon dielectric barrier discharge for excimer lamp," *IEEE Trans. Plasma Sci.*, vol. 42, no. 3, pp. 712–720, Mar. 2014.

[14] D. Florez, R. Diez, K. Hay, and H. Piquet, "DBD excimer lamp power supply with fully controlled operating conditions," in *Proc. 13th Int. Conf. Optim. Elect. Electron. Equip. (OPTIM)*, May 2012, pp. 1346–1352.

[15] H. Piquet, S. Bhosle, R. Diez, and M. V. Erofeev, "Pulsed current-mode supply of dielectric barrier discharge excilamps for the control of the radiated ultraviolet power," *IEEE Trans. Plasma Sci.*, vol. 38, no. 10, pp. 2531–2538, Oct. 2010.

[16] X. Bonnin, J. Brandelero, N. Videau, H. Piquet, and T. Meynard, "A high voltage high frequency resonant inverter for supplying DBD devices with short discharge current pulses," *IEEE Trans. Power Electron.*, vol. 29, no. 8, pp. 4261–4269, Aug. 2014.

[17] M. Amjad, Z. Salam, M. Facta, and S. Mekhilef, "Analysis and implementation of transformerless LCL resonant power supply for ozone generation," *IEEE Trans. Power Electron.*, vol. 28, no. 2, pp. 650–660, Feb. 2013.

[18] L. Chang, T. Guo, J. Liu, C. Zhang, Y. Deng, and X. He, "Analysis and design of a current-source CLCC resonant converter for DBD applications," *IEEE Trans. Power Electron.*, vol. 29, no. 4, pp. 1610–1621, Apr. 2014.

[19] M. Meißer, R. Kling, and W. Heering, "Transformerless high voltage pulse generators for bipolar drive of dielectric barrier discharges," in *Proc. PCIM Conf. Exhibit.*, May 2011, pp. 259–264.

[20] C. Monge-Dauge, F. Clement, P. Svarnas, J. Loiseau, A. Ricard, and B. Held, "Experimental study coupled with electrical modeling for the consideration of DBD-based plasma jet," *IEEE Trans. Plasma Sci.*, vol. 40, no. 9, pp. 2254–2260, Sep. 2012.

[21] X. Tang, Y. Yu, Z. Meng, and S. Li, "Study on an engineering design method for power supply of DBD type ozone generator," in *Proc. Chin. Autom. Congr. (CAC)*, Nov. 2013, pp. 713–717.

[22] R. Díez, J.-P. Salanne, H. Piquet, S. Bhosle, and G. Zissis, "Predictive model of a DBD lamp for power supply design and method for the automatic identification of its parameters," *Eur. Phys. J. Appl. Phys.*, vol. 37, no. 3, pp. 307–313, 2007.

[23] M. Cousineau, R. Diez, H. Piquet, and O. Durrieu, "Synthesized high-frequency thyristor for dielectric barrier discharge excimer lamps," *IEEE Trans. Ind. Electron.*, vol. 59, no. 4, pp. 1920–1928, Apr. 2012.

[24] D. Florez, R. Diez, H. Piquet, and K. Hay, "Square-shape current-mode supply for parametric control of the DBD excilamps power," *IEEE Trans. Ind. Electron.*, to be published, doi: 10.1109/TIE.2014.2361601.

[25] X. Bonnin, H. Piquet, N. Naudé, M. C. Bouzidi, N. Gherardi, and J.-M. Blaquière, "Design of a current converter to maximize the power into homogeneous dielectric barrier discharge (DBD) devices," *Eur. Phys. J. Appl. Phys.*, vol. 64, no. 1, pp. 10901–10908, Oct. 2013.

[26] R. Diez, H. Piquet, S. Bhosle, J.-M. Blaquiere, and N. Roux, "Design of a current converter for the study of the UV emission in DBD excilamps," in *Proc. IEEE Int. Symp. Ind. Electron. (ISIE)*, Jun./Jul. 2008, pp. 62–67.

[27] R. Diez-Medina, "Alimentation de puissance d'une lampe exciplexe à décharge à barrière diélectrique, en vue du contrôle du rayonnement," Ph.D. dissertation, Dept. Elect. Eng., INP Toulouse, Toulouse, France, Oct. 2008.

[28] R. Diez, H. Piquet, M. Cousineau, and S. Bhosle, "Current-mode power converter for radiation control in DBD excimer lamps," *IEEE Trans. Ind. Electron.*, vol. 59, no. 4, pp. 1912–1919, Apr. 2012.

[29] R. Diez, H. Piquet, S. Bhosle, and J.-M. Blaquiere, "Current mode converter for dielectric barrier discharge lamp," in *Proc. IEEE Power Electron. Specialists Conf. (PESC)*, Jun. 2008, pp. 2485–2491.

[30] D. Florez, R. Diez, and H. Piquet, "DCM-operated series-resonant inverter for the supply of DBD excimer lamps," *IEEE Trans. Ind. Appl.*, vol. 50, no. 1, pp. 86–93, Jan./Feb. 2014.

[31] D. Florez, X. Bonnin, R. Diez, and H. Piquet, "Impact of the transformer in the current mode supply of dielectric barrier discharge excimer lamps," in *Proc. Brazilian Power Electron. Conf. (COBEP)*, Oct. 2013, pp. 1171–1176.

[32] X. Bonnin, H. Piquet, R. Diez, and D. Florez, "Designing the high voltage transformer of power supplies for DBD: Windings arrangment to reduce the parasitic capacitive effects," in *Proc. 15th Eur. Conf. Power Electron. Appl. (EPE)*, Sep. 2013, pp. 1–9.

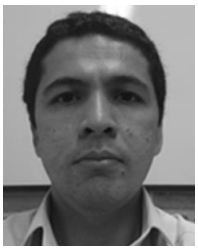

Rafael Diez (M'10) received the B.S. degree in electronics engineering from Pontificia Universidad Javeriana (PUJ), Bogotá, Colombia, in 2001, and the M.S. and Ph.D. degrees from the Université de Toulouse, Toulouse, France, in 2005 and 2008, respectively.

He is currently an Assistant Professor with the Department of Electronics, PUJ. His current research interests include the development of power converters for electric discharges.

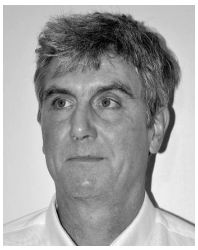

Hubert Piquet received the M.S. degree in applied physics from the École Normale Supérieure de Cachan, Cachan, France, in 1984, and the Ph.D. degree in electrical engineering from the Institut National Polytechnique de Toulouse, Toulouse, France, in 1990.

He is currently a Professor with the ENSEEIHT Engineering School, Institut National Polytechnique de Toulouse, where he teaches power electronics and is involved in research with the Laboratoire Plasma et Conversion d'Energie. His current research interests include quality and stability in embedded networks and power supplies for the electrical discharge applications.

David Florez (M'12) received the Electronics Engineering degree from Pontificia Universidad Javeriana (PUJ), Bogotá, Colombia, in 2005, the M.S. degree in critical systems and networks from Université Paul Sabatier, Toulouse, France, in 2006, and the Ph.D. degree from PUJ and the Institut National Polytechnique de Toulouse, Toulouse, in 2014.

He is currently a full-time Researcher and Professor with Universidad Sergio Arboleda, Bogotá, where he teaches courses on circuits and electronics. His current research interests include power converters and lighting.

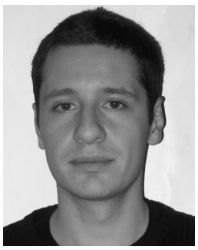

Xavier Bonnin was born in Clermont-Ferrand, France, in 1985. He received the M.S. degree in electrical engineering from the École Normale Supérieure de Cachan, Cachan, France, in 2011. He is currently pursuing the Ph.D. degree with the Laboratoire Plasma et Conversion d'Energie, Toulouse, France.

His current research interests include the study of the coupling between electrical power sources and plasma devices, and the methodologies in designing power electronics components for plasma applications.